

## Article

# Insights of Selective Catalytic Reduction Technology for Nitrogen Oxides Control in Marine Engine Applications

Pierpaolo Napolitano <sup>1</sup>, Leonarda Francesca Liotta <sup>2</sup>, Chiara Guido <sup>1</sup>, Cinzia Tornatore <sup>1,\*</sup>,  
Giuseppe Pantaleo <sup>2,\*</sup>, Valeria La Parola <sup>2</sup> and Carlo Beatrice <sup>1</sup>

<sup>1</sup> Istituto di Scienze e Tecnologie per l'Energia e la Mobilità Sostenibili (STEMS-CNR), Via Marconi 4, 80125 Napoli, Italy

<sup>2</sup> Istituto per lo Studio dei Materiali Nanostrutturati (ISMN-CNR), Via Ugo La Malfa 153, 90146 Palermo, Italy

\* Correspondence: cinzia.tornatore@stems.cnr.it (C.T.); giuseppe-pantaleo@cnr.it (G.P.)

**Abstract:** The international shipping industry is facing increasingly stringent limitations on nitrogen oxide (NO<sub>x</sub>) emissions. New solutions for reducing NO<sub>x</sub> emitted by marine engines need to be investigated to find the best technology. Selective Catalytic Reduction (SCR) is an advanced active emissions control technology successfully used in automotive diesel engines; it could be applied to marine engines with ad-hoc solutions to integrate it in the exhaust of large engines. In this study, a commercial SCR was tested at the exhaust of a diesel engine in inlet gas conditions typical of a marine engine. The SCR system consisted of a custom monolith (provided by Hug-Engineering AG) that enabled seamless integration for a broad range of engine sizes; the active phases were V<sub>2</sub>O<sub>5</sub> (3 wt%)-WO<sub>3</sub> (7 wt%)-TiO<sub>2</sub> (75 wt%). The monolith was studied at the laboratory scale for its in-depth chemical/physical characterization and by means of an intermediate-scale engine, reproducing the exhaust gas conditions of a full-scale marine engine. The system's effectiveness in terms of NO<sub>x</sub> removal for the selected engine operating conditions was evaluated in a wide range of temperature and NO<sub>x</sub> emissions values and for different quantities of the reduction agent (AdBlue or ammonia) added to exhaust gases. The investigated technological solution resulted in efficient NO<sub>x</sub> emission control from a marine engine.

**Keywords:** extruded monolith; V<sub>2</sub>O<sub>5</sub>-WO<sub>3</sub>-TiO<sub>2</sub>; SCR; ammonia; marine engine



**Citation:** Napolitano, P.; Liotta, L.F.; Guido, C.; Tornatore, C.; Pantaleo, G.; La Parola, V.; Beatrice, C. Insights of Selective Catalytic Reduction Technology for Nitrogen Oxides Control in Marine Engine Applications. *Catalysts* **2022**, *12*, 1191. <https://doi.org/10.3390/catal12101191>

Academic Editor: Zhaoyang Fan

Received: 2 September 2022

Accepted: 5 October 2022

Published: 8 October 2022

**Publisher's Note:** MDPI stays neutral with regard to jurisdictional claims in published maps and institutional affiliations.



**Copyright:** © 2022 by the authors. Licensee MDPI, Basel, Switzerland. This article is an open access article distributed under the terms and conditions of the Creative Commons Attribution (CC BY) license (<https://creativecommons.org/licenses/by/4.0/>).

## 1. Introduction

Marine diesel engines have always used heavy fuel oil, a poor-quality fuel that contains a high concentration of sulfur; therefore, among the pollutants produced, sulfur oxides (SO<sub>x</sub>) are of great importance, together with nitrogen oxides (NO<sub>x</sub>) and particulate matter (PM) [1]. Nitrogen oxides have a major impact on air pollution. They can damage the human respiratory system, promote secondary organic aerosols, acid rain and haze photochemical smog and contribute to ozone depletion [2]. NO<sub>x</sub> emissions from marine engines have been recently taken into consideration by the Tier III standards of the International Maritime Organization (IMO), introduced on January, 1st 2016 (MARPOL Annex VI). These regulations require an 80% reduction in NO<sub>x</sub> emissions compared to Tier I, and they apply in selected sea areas called "NO<sub>x</sub> Emission Control Areas (N-ECAs)" that comprise the coastal waters of the United States and Canada, the North Sea and the Baltic Sea. In addition to the IMO conventions, other maritime organizations such as the United States' Environment Protection Agency (EPA), the European Union and the Chinese Ministry of Environmental Protection have also established maritime regulations for the reduction in exhaust emissions [3].

Exhaust gas aftertreatment devices can efficiently remove pollutants from internal combustion (IC) engines' exhausts without a penalty in engine power and fuel economy. Among them, selective catalytic reduction (SCR) systems are widely adopted in road

applications for effectively reducing NO<sub>x</sub>. SCRs can operate as a standalone technology; they show high levels of reliability and durability, and they do not require major engine modifications. This technology includes an injection of urea water into the exhaust gas; taking advantage of the exhaust gas heat, ammonia (NH<sub>3</sub>) is produced through urea thermal decomposition. NH<sub>3</sub> reacts with NO<sub>x</sub> on a catalyst to convert NO<sub>x</sub> into molecular nitrogen (N<sub>2</sub>) and water (H<sub>2</sub>O). The main global reactions occurring in a SCR are presented in Table 1.

**Table 1.** Main global reactions occurring in an SCR.

NO <sub>x</sub> Reduction Reactions	Undesirable Oxidation Reactions
(a) $4\text{NO} + 4\text{NH}_3 + \text{O}_2 \rightarrow 4\text{N}_2 + 6\text{H}_2\text{O}$	(d) $4\text{NH}_3 + 5\text{O}_2 \rightarrow 4\text{NO} + 6\text{H}_2\text{O}$
(b) $6\text{NO}_2 + 8\text{NH}_3 \rightarrow 7\text{N}_2 + 12\text{H}_2\text{O}$	(e) $4\text{NH}_3 + 3\text{O}_2 \rightarrow 2\text{N}_2 + 6\text{H}_2\text{O}$
(c) $\text{NO} + \text{NO}_2 + 2\text{NH}_3 \rightarrow 2\text{N}_2 + 3\text{H}_2\text{O}$	(f) $2\text{NH}_3 + 2\text{O}_2 \rightarrow \text{N}_2\text{O} + 3\text{H}_2\text{O}$
	(g) $\text{SO}_2 + 1/2\text{O}_2 \rightarrow \text{SO}_3$

Reaction (a) represents the overall stoichiometry of the SCR process; it occurs rapidly in the presence of catalysts when the temperature is between 250 and 450 °C and oxygen is in excess. Usually, NO<sub>2</sub> concentration at the exhaust is very low (only 5% of the NO<sub>x</sub>), so reactions (b) and (c) play a minor role in the process.

As for the undesired oxidation reactions, those indicated with the letters d-f involve NH<sub>3</sub> consumption and determine a reversal of NO<sub>x</sub> removal and the formation of N<sub>2</sub>O as a by-product. These reactions can take place on SCR catalysts when the feed is low in NO, but they are negligible in the presence of NO<sub>x</sub>.

Ammonia has been chosen as reducing agent in the SCR process due to its capability to selectively react with NO<sub>x</sub> in excess of oxygen. This property is not observed in other simple reagents such as hydrocarbons and carbon monoxide. Reaction (g) is the oxidation of SO<sub>2</sub>, responsible for the formation of salts such as ammonium sulfate [4].

The core of the SCR technology is the catalyst system that has the role of improving the reaction efficiency by decreasing the activation energy and reaction temperature of NO<sub>x</sub> decomposition, increasing N<sub>2</sub> selectivity in NO<sub>x</sub> reduction products and preventing the incidence of side reactions. Selecting the appropriate catalysts is critical when designing an SCR; its main characteristics should be high deNO<sub>x</sub> activity, strong anti-poisoning ability, high mechanical strength and a suitable operating temperature range [5]. Many catalysts have been demonstrated to be effective in SCR reactions. Noble and transition metal oxides are the primary active components, with TiO<sub>2</sub>, Al<sub>2</sub>O<sub>3</sub>, SiO<sub>2</sub>, zeolite and carbon serving as carriers.

For low- and medium-speed marine engines, SCR technology is derived from power plant systems using diesel engines. While ammonia water can be used in power plants as a reducing agent, larger ships only use urea water solutions [6] for safety and storage reasons. The size of the urea-SCR system can also be an issue; the SCR urea consumption is estimated to be 8.5% of the diesel consumption [7]; this undoubtedly adds size and weight to the ship. Furthermore, the vibration resistance of urea tubes should be carefully considered. Pumping and dosing systems, as well as urea feed pipes, use welding connections whenever possible to avoid urea leaks [8].

Furthermore, the main challenges for marine SCR applications are low temperature sulfur resistance and low temperature activation. The latter issue is also a problem for cars, trucks and off-road applications and can result in the catalyst not working, for example at startup and during maneuvering [9]. In marine engines, the turbine downstream temperatures are generally below 150 °C, making catalytic exhaust gas treatment impossible. For this reason, the SCR catalyst is usually placed on top of the turbocharger close to the engine to allow the highest possible temperature for an efficient NO<sub>x</sub> conversion and to avoid the formation of ammonium sulfates. In this case, the system is called high-pressure SCR (HP-SCR) and it is mostly used for two-stroke low-speed diesel engines. HP-SCR is characterized by a compact layout and high exhaust gas energy utilization rate, but it

has a significant impact on the working performance of diesel engines and turbochargers. Conversely, an SCR arranged after the turbocharger is referred to as low-pressure SCR (LP-SCR). This system has high adaptability and a lower impact on the engine and turbocharger but its denitration efficiency is inadequate for low-speed two-stroke diesel engines because of the low exhaust temperatures. For this reason, an exhaust gas heating device is usually installed before the SCR reactor [10]. In the frame of the above literature, it emerges that the investigation of NO SCR catalysts for marine applications and the issues related to on-board installation deserve further efforts. Some numerical investigations have recently been performed to predict the denitration efficiency, ammonia flow rate and other parameters of SCR systems for marine applications [11,12]; less effort has been made for experimental studies.

Most catalysts for marine SCRs are  $V_2O_5$ - $WO_3$ - $TiO_2$ -based; vanadium and tungsten oxides coated on a titanium substrate [13].  $V_2O_5$  is the active component (1–3%), which is usually impregnated on an anatase  $TiO_2$  support together with  $WO_3$  (~10%) to stabilize the vanadia and increase thermal durability. The typical maximum  $NO_x$  conversion range is between ~250 °C and ~450–500 °C. Above this temperature, selectivity is reduced because  $NH_3$  is oxidized by  $O_2$  instead of reacting with NO [14]. A  $V_2O_5$ - $WO_3$ - $TiO_2$  SCR is commonly used as a stationary catalyst, but it has not been commercialized for vehicles due to vanadium toxicity. Conversely, this type of SCR catalyst is appropriate for ships because of its high light-off efficiency, good sulfur resistance and low cost, so its demand in the market has increased.

It is worth noting that zeolite-based catalysts can also be effective in catalytic exhaust gas aftertreatment systems because they are characterized by a high specific surface area and thermal stability. In recent years, many studies have improved the de- $NO_x$  performance and durability of Cu-zeolite catalysts that show excellent low temperature activity [15–18]. Fe-zeolite has great durability toward high temperature and poisoning; thus, it can be successfully used in after-treatment catalysts for heavy-duty diesel engines even if it shows a high activation energy, causing low light-off performance.

Some researchers have compared  $V_2O_5$ - $WO_3$ - $TiO_2$  catalysts [19] with two kinds of Fe-zeolite (Fe-zeolite (1) and (2)). Their physicochemical characteristics were examined according to hydrothermal aging, sulfur poisoning and HCs co-existence. The results showed that  $V_2O_5$ - $WO_3$ - $TiO_2$  SCR was the least susceptible to sulfur poisoning because of Brønsted acid site effects and its  $NO_x$  conversion rate was relatively higher at ~350 °C. It resulted in being the most suitable for the reduction in exhaust gas from ship engines.

Magnusson et al. [12] investigated how sulfur, water and low temperature affect  $NO_x$  the reduction activity of a commercial SCR  $V_2O_5$ - $WO_3$ - $TiO_2$  catalyst in marine applications using urea as a reducing agent. The authors proved that for temperatures higher than 300 °C,  $NO_x$  reduction could be greater than 90%. Japke et al. [20] tested the performance of vanadia-based SCR catalysts obtained using the incipient wetness impregnation method. The study demonstrated that the preparation process had a strong effect on the catalyst's  $NO_x$  removal efficiency with ammonia and on the oxidation activity of soot and hydrocarbons. Zhou et al. [21] studied the catalytic activities of an extruded commercial monolithic  $V_2O_5$ - $WO_3$ - $TiO_2$  catalyst at low temperatures according to the working characteristics of marine diesel engines. The authors reported that for temperature below 150 °C, the SCR reaction was mostly influenced by internal chemical reaction kinetics, and when the temperature was above 200 °C, the most relevant mechanism affecting the SCR reaction was the reactant diffusion rate. The parameters that can improve  $NO_x$  reduction were found to be space velocity,  $NH_3$  consumption and  $O_2/NO_2$  concentration in the gas mixture.

Recently, Lai et al. [22] and Zhang in collaboration with some authors of the present paper [23] have pointed out that the catalyst's preparation method, the titania surface area and crystalline structure, the vanadium and tungsten loadings and the calcination treatments strongly affect the morphological, structural, acidic properties and NO SCR performance.

The unequivocal result emerging from all the studies is the crucial role played by the titania support with the capability to establish a proper interaction of the  $V_2O_5$  and  $WO_3$  active phases. Moreover, the shape and nature of the monolith, as extruded or wash-coated by the active phases, and its manufacturing procedure are undoubtedly key factors.

On these bases, we considered an extruded monolithic catalyst worthy of investigation, provided by Hug Engineering AG (Elsau-Switzerland) containing  $V_2O_5$  (3 wt%)- $WO_3$  (7 wt%)- $TiO_2$  (75 wt%), rest bentonite and glass fiber as the active phases. Such a catalytic device that normally is used for the abatement of  $NO_x$  from stationary sources was firstly characterized in terms of its physical-chemical properties at laboratory scale. Then, it was installed and tested at the exhaust of a diesel engine in exhaust conditions representative of a marine on-board power generation engine. This kind of engine was equipped with high-pressure common rail injection systems and worked with low-sulfur diesel fuel (EN590).

The adopted methodology led to an assessment of the applicability and potentiality of the system when installed on a real engine, enlarging the scientific literature with quantitative data and information. Once the good potentiality of the system was revealed, the next step of investigation regarded the analysis of other aspects important for a future installation at the exhaust of marine engines, i.e., the poisoning resistance of the system and its thermal management. An experimental/numerical approach will be useful to enlarge the systems working conditions.

The results presented in this study are part of a wider project devoted to investigating low-impact technology solutions for power generation in marine applications.

## 2. Experimental Setup and Procedures

The methodology approach foresaw two different steps of investigation.

The study was initially conducted for a complete characterization of the physical-chemical properties. In this sense, the catalytic system was analyzed, as slab and/or as powder, in terms of the crystalline structure of the monolithic catalyst, specific surface areas, pore volume, pore size of the material, reduction properties and surface composition by means of proper diagnostics techniques.

The second step consisted of investigating the potentiality offered by the same SCR on an intermediate-scale engine, reducing the complexity of a test campaign on a real-scale marine engine. The experimental procedure foresaw to firstly assess the representativeness of the intermediate-scale engine, identifying test conditions typical of a real use of an SCR. Then, a monolith, representing one element of a full-scale SCR, was installed at the exhaust of the intermediate-scale engine and was characterized in terms of its  $NO_x$  reduction efficiency.

The aim of such a research approach was to guarantee an in-depth analysis of the monolith potentiality, correlating the monolith features with its measured performance. The two laboratory experimental set-ups, the adopted diagnostic techniques and instrumentation are described in the following sections.

### 2.1. Laboratory Scale

The SCR device, provided by Hug Engineering AG, had a monolithic structure, 200 cpsi and a geometric parallelepiped shape. The chemical composition, as certified in the data sheet, is listed in Table 2.

**Table 2.** Chemical composition of the monolithic catalyst.

Phase	Wt%
$TiO_2$	75.0
$WO_3$	7.0
$V_2O_5$	3.0
bentonite	6.0
glass fiber	9.0

The crystalline structure of the catalyst (as a slab and as a powder) was determined by powder X-ray diffraction patterns (XRD), performed on a Bruker D5000 diffractometer equipped with a Cu K $\alpha$  anode and graphite monochromator. The data were recorded in a  $2\theta$  range of 20–80° with a step size of 0.05° and time per step of 20 s. Moreover, a pattern with an acquisition time of 200 s/step was registered between 20 and 60°  $2\theta$  to confirm the absence of peaks ascribable to the V<sub>2</sub>O<sub>5</sub> and/or WO<sub>3</sub> phases. The only detected crystalline phases attributed to TiO<sub>2</sub> were analyzed according to ICSD files (Inorganic Crystal Structure Database). The mean crystallite size was calculated by the Debye–Scherrer equation:  $D = 0.9\lambda/B\cos\theta$ , where  $D$  represents the average crystalline size, 0.9 is the Scherrer parameter,  $\lambda$  is the wavelength of the X-ray radiation (0.15406 nm),  $B$  denotes the full width at half maximum of the peak (FWHM) and  $\theta$  is the angular position of the peak.

The specific surface areas (SSA), pore volume and pore size of the material (as a slab and as a powder) were measured by N<sub>2</sub> adsorption–desorption isotherms using a Micromeritics ASAP2020 system. Before analysis, the samples were degassed in vacuum at 250 °C for 2 h, then the measurement was performed at liquid nitrogen temperature (−196 °C). The Brunauer–Emmett–Teller (BET) method was used to calculate the SSA. The Barrett–Joyner–Halenda (BJH) method [24] was applied to the desorption branch to estimate the pore volume and pore size distribution.

The catalyst (0.1 g), as a powder, was studied by hydrogen temperature-programmed reduction (H<sub>2</sub>-TPR) using Micromeritics Autochem 2910 HP apparatus equipped with a thermal conductivity detector (TCD). The H<sub>2</sub>-TPR profiles were registered after pre-treatment under O<sub>2</sub>/He flow from room temperature up to 300 °C with a holding time of 30 min. Then, after cooling down up to RT under He flow, the H<sub>2</sub>-TPR analysis was carried out in the temperature range of 25–1000 °C with a 10 °C min<sup>−1</sup> heating rate and a flowing 5 vol.% of H<sub>2</sub> in Ar (30 mL/min).

The X-ray photoelectron spectroscopy (XPS) analyses of the samples were performed with a VG Microtech ESCA 3000 Multilab (VG Scientific, East Grinstead, UK), using unmonochromatized Al K $\alpha$  source (1486.6 eV) run at 14 kV and 15 mA and a CAE (Constant Analyser Energy) mode. A pass energy of 50 eV set across the hemispheres was used for the survey spectrum, and a value of 20 eV was used for the individual peak energy regions pass energy. The constant charging of the samples was removed by referencing all the energies to the C1s peak energy set at 285.1 eV, arising from adventitious carbon. Analyses of the peaks were performed using the CASA XPS software (version 2.3.17, Casa Software Ltd., Wilmslow, UK, 2009). For the peak shape, a Gaussian (70%)–Lorentzian (30%) line shape defined in Casa XPS as GL (30) profiles were used for each component of the main peaks after a Shirley type baseline subtraction. The binding energy values were quoted with a precision of  $\pm 0.15$  eV and the atomic percentage with a precision of  $\pm 10\%$ .

## 2.2. Engine Intermediate Scale

The final application of the prototype after-treatment device will be a marine engine, i.e., an ISOTTA FRASCHINI (IF) 4-stroke, water-cooled 8-cylinder V engine with 2 intake and 2 exhaust valves. The rated speed and power are 1500 rpm and 685 kW, respectively. The engine is equipped with a common rail injection system with electronic control and variable injection timing. The unit displacement is 3856.7 cm<sup>3</sup> and the nominal compression ratio is 13.2.

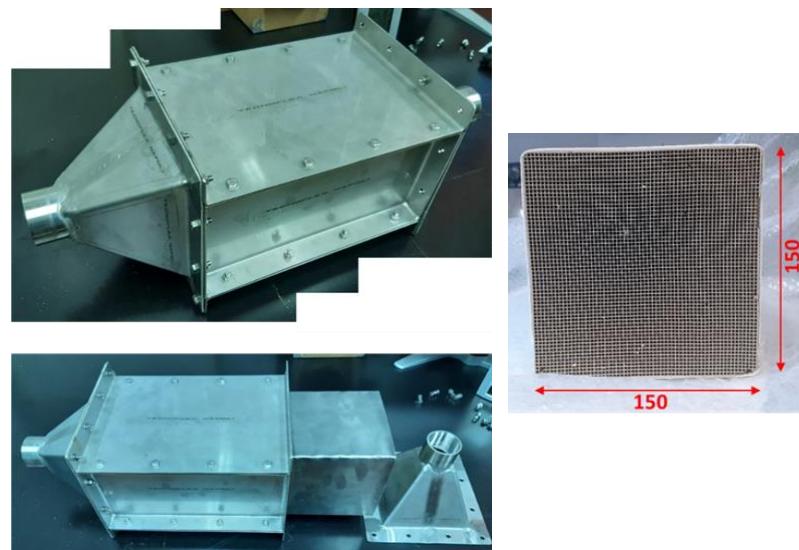
Nevertheless, considering the size of the naval engine and the complexity and costs of the test campaign that would result, the characterization of the prototype after treatment device was carried out on an intermediate-scale (IS) engine; a heavy-duty engine for truck or bus applications, its main specifics are presented in Table 3.

**Table 3.** IS engine main technical characteristics.

<b>Heavy-Duty Engine for Truck Application</b>	
Type	Straight-four
Bore × Stroke	104 mm × 103 mm
Total displacement	4483 cm <sup>3</sup>
Compression ratio	17.1:1
Maximum power	152 kW @ 2500 rpm
Maximum torque	750 Nm @ 1600 rpm
Minimum idle speed	750 rpm
Maximum idle speed	3000 rpm

The IS engine was compliant with the latest anti-pollution regulations for road vehicles used in truck or bus applications (EURO VI). It was equipped with an after-treatment system consisting of a diesel oxidation catalyst (DOC), particulate filter (DPF) and nitrogen oxide catalyst (SCR). All these components were engineered in a single compact unit and real-time controlled by the engine control unit to ensure its efficient operation in the various working conditions. The engine was installed on a dyno test bench and instrumented for pressure and temperature characterization both at the intake and exhaust line.

At the engine exhaust, a smoke meter was used for smoke emission measurement, while the regulated gaseous emissions (THC, CO, CO<sub>2</sub>, NO<sub>x</sub>/NO, O<sub>2</sub>) were measured upstream and downstream of the aftertreatment system with an exhaust gas analyzer bench (Horiba Mexa 7100). The parallelepiped-shaped SCR prototype was housed in the box shown in Figure 1, which was custom designed.

**Figure 1.** Box and monolith.

The engine exhaust line (originally providing a standard ATS layout) was properly modified to allow the SCR device installation. According to the scheme of Figure 2, the exhaust gas downstream of the turbine was driven to the new device by capping the original exhaust duct output.

The monolith had the following sizes: 150 × 150 × 300 mm and a volume of 6.75 dm<sup>3</sup>. The single monolith represented one of the twenty “bricks”, of which the catalyst for the reference marine engine should be constituted. This solution, although different from the typical layouts for road applications (cylindrical), could be the most suitable for a large and perhaps modular naval application.

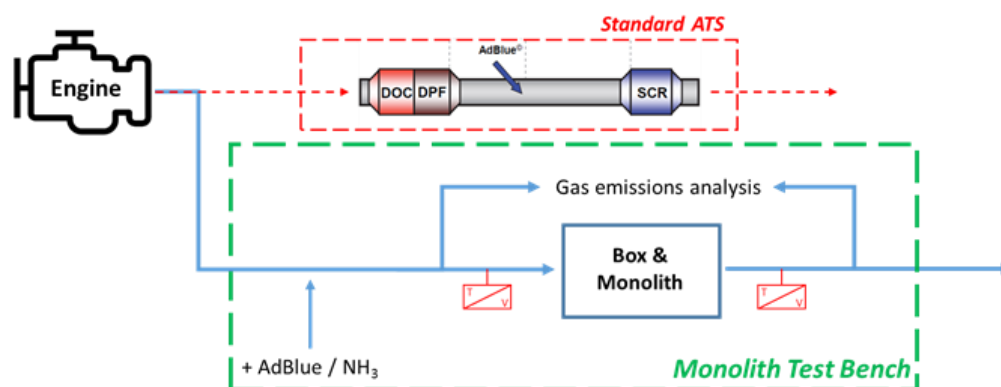


**Figure 2.** Diagram of the test bench for prototype SCR devices.

To stabilize the flow of exhaust gases and direct them to each part of the monolith, a connecting section with an exhaust manifold was designed. Due to the high temperature of the exhaust gases and to ensure the least interference from a chemical point of view with the gas stream, the whole exhaust line was made of stainless steel. The monolith box could be completely disassembled; this ensured easy and safe installation and replacement of the prototype to be characterized. For the SCR operation, a solution of water and urea was continuously nebulized in the exhaust gas stream; a standard urea injection system was used, consisting of an AdBlue tank, dosing unit, pressurization unit and an injector positioned along the exhaust duct. The injector actuation was controlled by the engine control unit and the AdBlue quantity could be properly dosed. In this way, it was possible to characterize the prototypes not only with respect to the quality of the exhaust gas ( $\text{NO}_x$  concentration and temperature, which varied according to the engine point) but also to the concentration of reducing agent.

The test bench was equipped with the following sensors:

- A thermocouple mounted at the entrance of the box to monitor the temperature of the inlet exhaust gases;
- A thermocouple mounted at the outlet of the box to evaluate the temperature variation in the exhaust gases that cool down flowing through the SCR;
- Exhaust gas sampling outlets “upstream” and “downstream” of the SCR to characterize the gas composition.

In a preliminary phase of this activity, the exhaust of the IF marine engine was characterized in the operating conditions representative of its standard working map in terms of flow rates, temperatures, gaseous pollutants and particulate matter concentrations, with the aim of subsequently reproducing such conditions at the exhaust of the intermediate-scale engine. E2/D2 test cycles were performed in controlled ambient conditions for five operating modes at a fixed speed of 1500 rpm and with torque values between 10 and 100%. The concentration of  $\text{NO}_x$ , CO,  $\text{CO}_2$ , THC, smoke and the thermodynamic properties of the exhaust gases were measured. Starting from this analysis, the first part of the experimental activity was aimed at the identification of five IS engine test points characterized by the same exhaust line conditions found during the above-described operation of the marine engine. Then, the experiments were focused on the characterization of the SCR prototype at the engine exhaust in the selected conditions.

### 3. Results and Discussion

#### 3.1. Characterization of the Monolith

In order to investigate the crystalline structure of the monolithic catalyst, XRD patterns were registered on the powder and as well on the slab, for comparison. In Figure 3a, the diffractogram registered for the powder, in the angular range  $20\text{--}80^\circ 2\theta$ , with a typical acquisition time of 20 s/step is shown. Only peaks of the anatase phase were identified by comparison with the ICSD reference of anatase (n. 9852, tetragonal, space group I

41/amdS), which is also displayed in the diffractogram. Similar results have been reported in previous work by some of the authors of this paper [25].

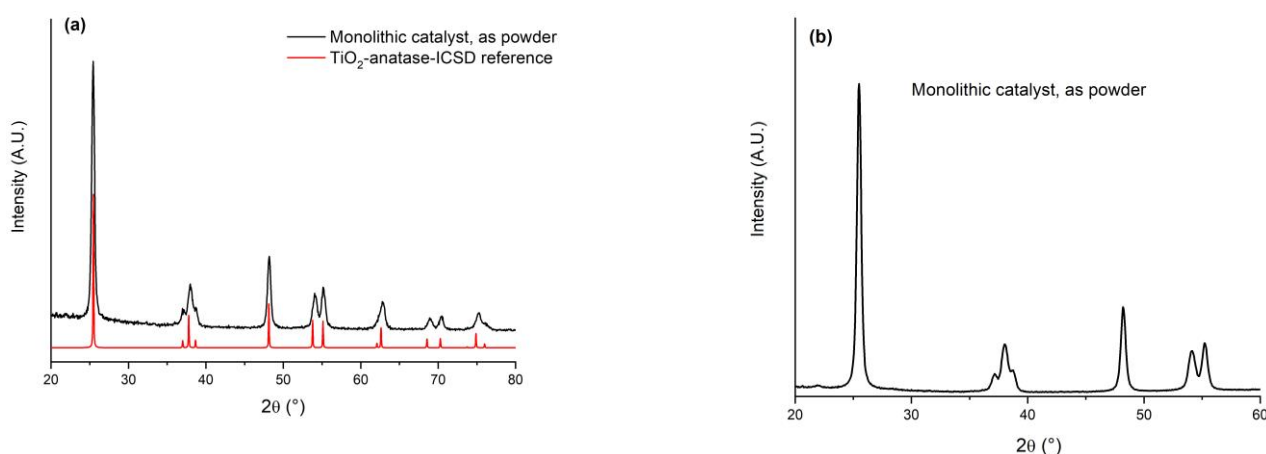


**Figure 3.** XRD patterns of the monolithic catalyst (as a powder) registered with different acquisition times: (a) 20 s/step; (b) 200 s/step. The TiO<sub>2</sub> anatase ICSD reference is plotted for comparison.

The absence of peaks ascribable to the WO<sub>3</sub> and V<sub>2</sub>O<sub>5</sub> phases was confirmed by recording a more detailed pattern with an acquisition time of 200 s/step in a selected angular range, between 20 and 60° 2θ (see Figure 3b), over a different portion of the powder. Identical XRD patterns showing only anatase peaks were obtained over the slabs of the monolith, confirming that the sample orientation did not affect the crystalline phases detectable. According with the literature, the absence of other crystalline phases, except those of TiO<sub>2</sub>, suggested the presence of WO<sub>3</sub> and V<sub>2</sub>O<sub>5</sub> as highly dispersed oxides or in an amorphous state. However, we cannot exclude that oxo-tungstate and V-O-W species were formed by the interaction of vanadium and tungsten with the support [26,27].

N<sub>2</sub> adsorption/desorption isotherms were registered over the monolithic sample, as a powder and as slab pieces, to measure the specific surface area (SSA), pore size distribution and pore volume. The values are listed in Table 4 and showed a good correspondence for the two sets of data. In both cases, an SSA value around 56 m<sup>2</sup>/g was measured, which is typical of pure TiO<sub>2</sub>, such as Evonik P25 [28], with a mean pore size of ~15 nm and pore volume 0.21 cm<sup>3</sup>/g. However, differently from TiO<sub>2</sub> P25, which is characterized by anatase and rutile phases, in the present monolith only anatase was detected (see Figure 3).

**Table 4.** Textural properties of the monolithic catalyst.

Sample	SSA (m <sup>2</sup> /g)	Mean Pore Diameter (nm) BJH Method *	BJH Pore Volume * (cm <sup>3</sup> /g)
Monolithic catalyst as a slab	56.0	14.8	0.21
Monolithic catalyst as a powder	55.6	15.0	0.21

\* The BJH method was applied to the desorption branch.

The reduction properties of the monolithic catalyst, as a powder, were investigated by H<sub>2</sub>-TPR analysis. A typical reduction profile registered for the monolith is displayed in Figure 4. According to the literature [21], the main peak centered at 471 °C was ascribed to the reduction of V<sup>5+</sup> to V<sup>3+</sup> corresponding to vanadia species highly dispersed over the titania surface, while the shoulder at 410 °C could be due to polymeric aggregates. Based on other investigations [29], intermediate oxides are formed during the reduction of V<sub>2</sub>O<sub>5</sub> to V<sub>2</sub>O<sub>3</sub> that could explain the asymmetric shape of the low temperature peak. By increasing the temperature, the reduction in mixed V-O-W species occurred at 635 °C, and then the broad peak at 852 °C was attributed to the reduction of W<sup>6+</sup> to W<sup>4+</sup> [21] or even to W<sup>0</sup> according to other authors [30].

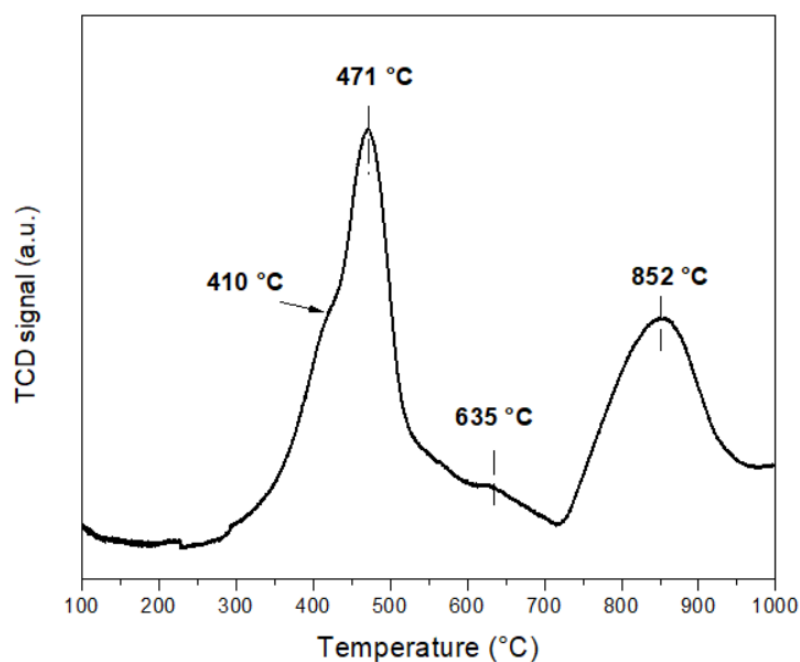


**Figure 4.** H<sub>2</sub>-TPR curve of monolith catalyst as a powder.

In Table 5, the hydrogen consumption values and the range of temperatures of the main peaks are reported. The experimental values are compared with the theoretical ones expected for the reduction of V<sub>2</sub>O<sub>5</sub> to V<sub>2</sub>O<sub>3</sub> and for the reduction of WO<sub>3</sub> to WO<sub>2</sub>/W<sup>0</sup>, calculated based on the V<sub>2</sub>O<sub>5</sub> and WO<sub>3</sub> wt% of the monolithic catalyst (see Table 2).

**Table 5.** Experimental H<sub>2</sub> consumption values derived from TPR, comparison with theoretical data.

Sample	T (°C)	Experimental H <sub>2</sub> Consumption (mL/g)	Theoretical H <sub>2</sub> Consumption (mL/g)
Monolithic catalyst as powder	300–700	14.8	8.1 (V <sub>2</sub> O <sub>5</sub> to V <sub>2</sub> O <sub>3</sub> )
	700–1000	17.3	7.4 (WO <sub>3</sub> to WO <sub>2</sub> ) 22.2 (WO <sub>3</sub> to W <sup>0</sup> )

Based on the values listed in Table 5, it can be deduced that the reduction of V<sub>2</sub>O<sub>5</sub> to V<sub>2</sub>O<sub>3</sub> was completed and, since the experimental consumption of 14.8 mL/g exceeded the theoretical one of 8.1 mL/g, it was expected that below 700 °C the reduction of some W also occurred, likely as mixed V-O-W species. At T > 700 °C, the consumption values of 17.3 mL/g suggest the occurrence of the reduction WO<sub>3</sub> to W<sup>0</sup>, although in the extent of V and W reduction, we must keep in mind that some surface (at around 300–500 °C) and bulk reduction (at around 850–900 °C) of TiO<sub>2</sub> took place [31].

The XPS analysis was performed on the monolithic catalyst as a slab in order to analyze the surface composition. Figure 5 shows the survey scan of the sample. The spectrum confirmed the presence of Ti, O, W, Si and Al according to the chemical composition, as reported in the data sheet. The main peak relative to vanadium (V2p) overlapped with the more intense O1s satellites arising from the K<sub>α3</sub>, so it was not visible in the survey spectrum and its analysis was subjected to an important error (see blue inset, Figure 5). On the contrary, the region between 30 and 50 eV contained peaks relative to W4f, Ti3p and V3p, which were clearly distinguishable, so this region was used to analyze and quantify these elements. The results in terms of W4f7/2, V3p and O1s binding energies (eV) and surface W/Ti and V/Ti atomic ratios are listed in Table 6. Figure 6 shows the W4f, Ti3p and V3p region of the monolith. The spectrum showed a complex peak, which could be deconvoluted with two doublets due to the spin orbit splitting of W4f7/2 and W4f5/2 (spin orbit separation = 2.1 eV, W4f7/2–W4f5/2 area ratio of 0.75), along with a peak attributed

to Ti3p and a peak due to V3p. According to the literature, the position of W4f7/2 of 35.5 eV was due to W(VI) while the W4f7/2 value of 34.3 eV was due to W(V) [32–34]. By deconvolution of the region, it was found that Tungsten was present mainly as W(VI) with a 10% presence as W(V). The V3p position was in accordance with the presence of V(V) [35–37]. Ti3p (37.2 eV) was in accordance with the presence of Ti(IV) [38,39]. This fact was confirmed by the analysis of the Ti2p region with the typical two peaks at 458.2 eV (Ti2p3/2) and 463.9 eV (Ti2p1/2), see the red inset of Figure 5 [40]. Oxygen showed the typical profile of the TiO<sub>2</sub> material with a component at ca. 529.5 eV due to its lattice and a component at 531.5 eV due to OH surface groups [35]. In Table 6, the surface atomic ratios of W/Ti and V/Ti are compared with the bulk values, derived from the real chemical composition as reported in Table 2. With respect to the calculated bulk values, the surface of the slab results was enriched in vanadium.

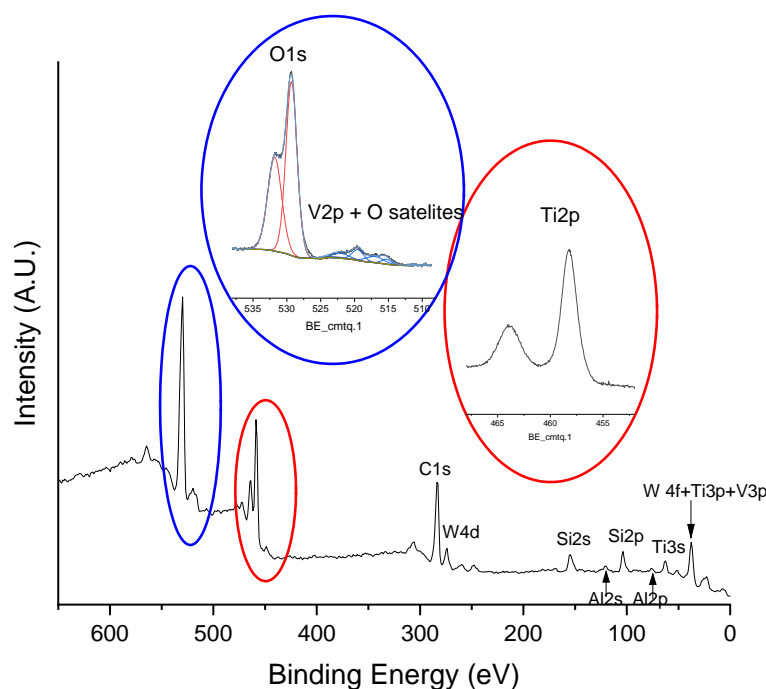


**Figure 5.** XPS survey spectrum of the monolithic catalyst (as a slab). The blue inset is the O1s + V2p region, the red inset is the Ti2p region.

**Table 6.** XPS results in terms of W4f, V3p and O1s binding energies (eV) of the monolithic device and W/Ti and V/Ti atomic ratios. The relative intensities of the different components of V and O are given in parentheses.

Sample	W4f7/2 (eV)	V3p eV	O1s	W/Ti (0.03) *	V/Ti (0.02) *
CM	34.3 (10%)	41.0	529.3 (57%)	0.03	0.14
	35.5 (90%)		531.8 (43%)		

\* Nominal ratio values.

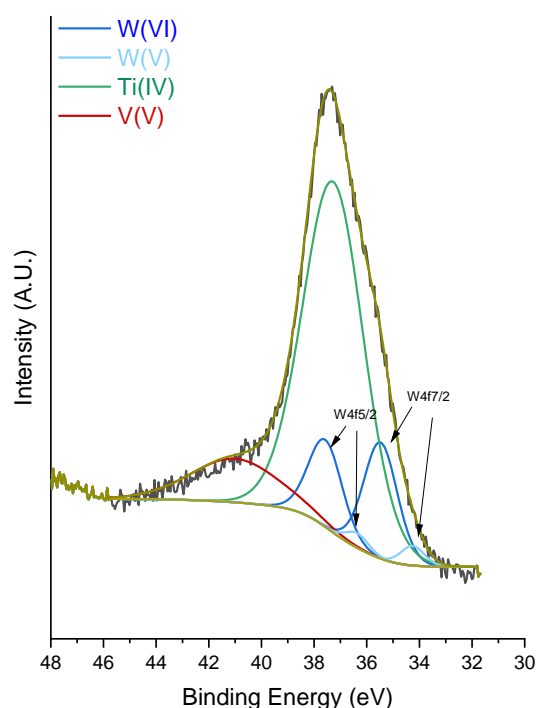


**Figure 6.** W4f, Ti3p and V3p region.

### 3.2. Monolith Performance at the Engine Exhaust

#### 3.2.1. Selection of the Engine Conditions

In the first phase of the experimental campaign, five operating points (modes) of the intermediate-scale engine were chosen considering the following constraints with respect to the corresponding IF mode:

- Exhaust flow scaled by 1/20;
- Equal exhaust gas temperatures downstream of the turbine;
- Same NO<sub>x</sub> concentration values;
- Same O<sub>2</sub> and CO<sub>2</sub> concentration values;
- Same air/fuel ratio.

The five intermediate-scale engine operating points, selected according to the experimental comparison between the two exhausts, are listed below, briefly indicated with the relative rotation speed (in rpm) and torque (in Nm):

Mode 1 1400 × 280

Mode 2 1200 × 170

Mode 3 1100 × 130

Mode 4 1000 × 80

Mode 5 900 × 20

The following figures report the comparison between the two engines behavior during the performed tests to demonstrate the reproducibility of the IF engine exhaust conditions in the intermediate-scale engine.

Tests repetitions were performed, and the standard deviation among all the IS tests is reported as error bars.

In Figure 7, the results obtained with the intermediate-scale (IS) engine in terms of NO<sub>x</sub> emissions (a) and exhaust gas temperatures (b) are compared with the corresponding results of the IF engine in the five selected operating points. The exhaust gas temperature was measured downstream of the turbine through a K-type thermocouple.

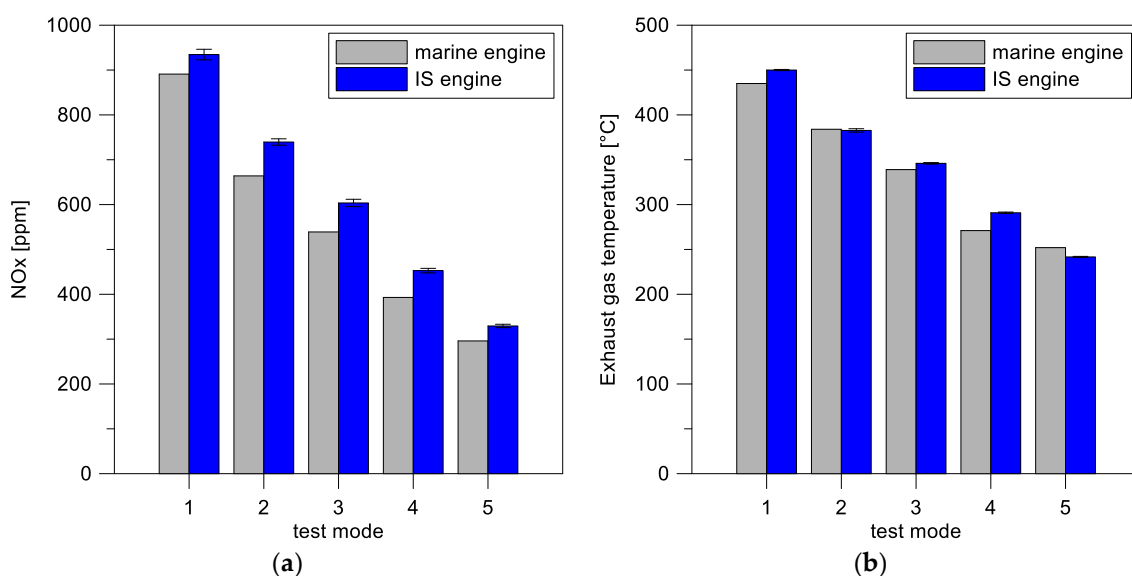


**Figure 7.** Comparison of (a) NO<sub>x</sub> and (b) exhaust temperatures between marine and intermediate-scale engine in the five selected modes.

The test points selected for the IS engine ensured exhaust gas conditions capable of reproducing the NO<sub>x</sub> concentrations and temperature values measured at the engine exhaust of the full-scale marine engine. In this way, it can be assumed that the study of the reduced-scale SCR system was representative of the full-scale one since the concentration of nitrogen oxides and the exhaust gas temperature are the two main parameters that influence the efficiency of an SCR device.

Figure 8a shows the comparison between the two engines in terms of exhaust gas flow rates and lambda, or  $(A/F)/(A/F)_{\text{stoichiometric}}$ . The exhaust gas flow rate of the intermediate-scale engine was compared with the real one, scaled by a ratio of 1:20. The corresponding O<sub>2</sub> and CO<sub>2</sub> emissions are reported in Figure 8b.

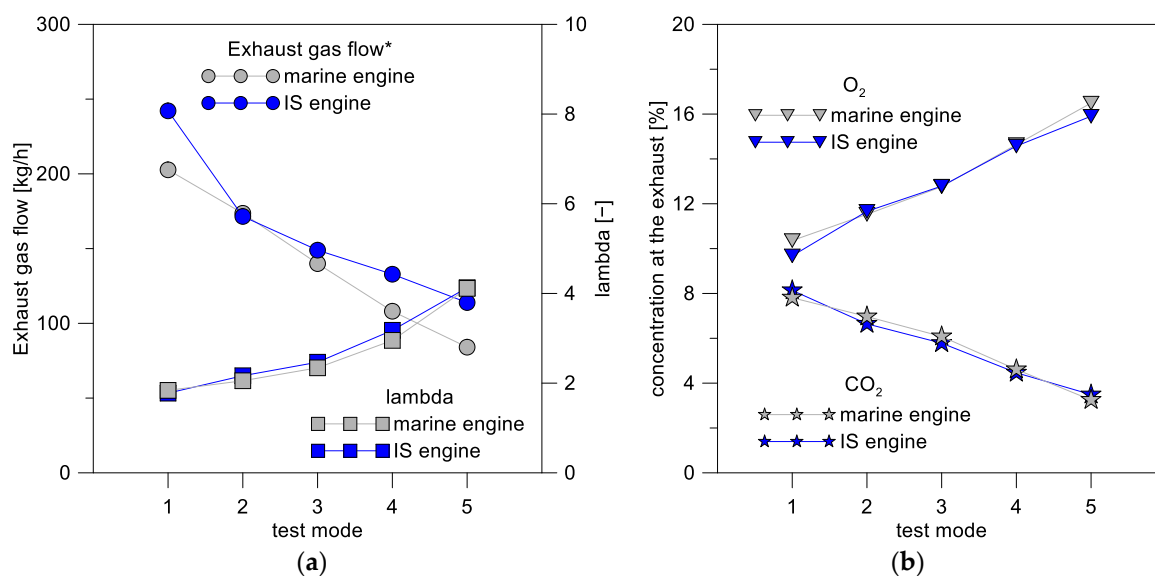


**Figure 8.** Comparison of (a) exhaust flow rate and lambda value and (b) O<sub>2</sub> and CO<sub>2</sub> emissions, between marine and intermediate-scale engine in the five selected modes. \* Note: for the marine engine, the gas flow is scaled 1:20.

The described comparison clearly highlights a good agreement between the IF-marine and the IS engines with respect to the trends of the selected quantities in all five investigated conditions.

The range of variability of the different quantities of interest was well reproduced and therefore the chosen operating modes could be used for the characterization of the prototype monolith catalysts.

The results also showed that the selected operating points allowed the characterization of the catalyst in a wide range of NO<sub>x</sub> concentration values ranging from 300 ppm to 900 ppm.

### 3.2.2. Tests for Monolith Characterization

A mixture of deionized water and urea AdBlue (approximately 67.5% water and 32.5% urea) was used as reducing agent and it was injected upstream of the steel case containing the monolith. The response of the AdBlue injector to the actuation command coming from the engine control unit was verified.

Based on the NO<sub>x</sub> concentration measured at the exhaust, a calculation was implemented that allowed the proper dosing of the amount of reducing agent to obtain a preset NH<sub>3</sub>/NO ratio (dosing ratio). The dosing ratio was indicated as a dimensionless factor “phi” that was equal to the ratio between the moles of NH<sub>3</sub> introduced into the exhaust gas flow and the moles of NO (phi = NH<sub>3</sub>/NO).

In more detail, the AdBlue quantity for a fixed phi value was obtained from the exhaust mass flow and the engine-out NO concentration values by means of the following formula, considering that in the thermal hydrolyzation of urea, each mole of urea decomposes to form two moles of ammonia [41]:

$$\text{phi} = \frac{0.5 \times n_{\text{UREA}}}{M_{\text{exh}} \times (x_{\text{NO}}/MW_{\text{exh}})} = \frac{0.5 \times (M_{\text{AdBlue}}/MW_{\text{UREA}}) \times \% \text{UREA}}{M_{\text{exh}} \times (x_{\text{NO}}/MW_{\text{exh}})} \quad (1)$$

where:

$n_{\text{UREA}}$  is the moles of urea

$x_{\text{NO}}$  is the NO concentration at the exhaust

$MW_{\text{exh}}$  is the average molecular weight of exhaust gas

$MW_{\text{UREA}}$  is the molecular weight of urea

$M_{\text{exh}}$  is the exhaust mass flow

$M_{\text{AdBlue}}$  is the AdBlue injection quantity

The Phi factor varied from 0, corresponding to no AdBlue injected, up to a value slightly higher than the stoichiometric one, i.e., the value corresponding to the quantity of NH<sub>3</sub> necessary for the complete reduction of all NO moles (phi = 1).

Table 7 shows the main parameters of interest to characterize the functional response of the monolith in the five selected modes.

**Table 7.** Operating conditions for the characterization of the monolith.

Mode	rpm × Nm	T <sub>Turbine out</sub> /T <sub>SCR in</sub> [°C]	O <sub>2</sub> , Engine Out [%]	NO <sub>x</sub> , Engine Out [ppm]	Space Velocity (SV) [h <sup>-1</sup> ]	phi = NH <sub>3</sub> /NO
1	1400 × 280	450/410	10	935	56,840	0; 0.2; 0.4; 0.7; 1.0; 1.1; 1.2
2	1200 × 170	380/340	12	740	39,957	0; 0.2; 0.4; 0.7; 1.0; 1.2
3	1100 × 130	345/300	13	604	34,071	0; 0.2; 0.4; 0.7; 1.0; 1.2
4	1000 × 80	290/245	15	453	27,947	0; 0.2; 0.4; 0.7; 1.0; 1.2
5	900 × 20	240/200	16	329	22,135	0; 0.4; 0.7; 1.0; 1.2

The temperatures were reported at the turbine outlet and in the immediate entrance to the SCR; their values ranged from 200 °C in mode 5 to 450 °C in mode 1, characterized by the lowest and the highest load, respectively. For the catalyst activity, higher temperatures are preferable to lower ones.

The concentrations of O<sub>2</sub> and NO<sub>x</sub> at the engine out, shown in the table, corresponded to the intake of the SCR.

The space velocity (SV) was calculated in the five selected operating conditions as the ratio between the volumetric flow velocity of gas passing in the monolith and the volume of the monolith. The higher the SV, the shorter the contact time between the catalyst and reactant molecules. Thus, a lower SV favors the yield of the reaction that takes place in the monolith. In the investigated conditions, the SV varied in a range of 22,135–56,840 h<sup>-1</sup>.

For each analyzed mode, a precise and unique combination of space velocity, NO<sub>x</sub> concentration, exhaust gas temperature and O<sub>2</sub> concentration was realized. Clearly, they were non-independent parameters, which balanced among themselves as in the commercial marine engine.

For each test mode, the characterization of the prototype monolith was carried out for different phi values; the column of Table 7 summarizes the dosing conditions tested in correspondence with the different engine modes.

During the test, the exhaust gas temperature and NO<sub>x</sub> concentration were measured upstream and downstream of the monolith. The reduction efficiency of the nitrogen oxides was calculated for the different concentrations of reducing agent.

Figure 9a shows the temperature measured upstream and downstream of the monolith versus phi in the five modes. The heat insulation allowed the keeping of very low heat losses to the outside and ensured a uniform temperature of the monolith during the test, as shown by the slight reduction between the upstream and downstream temperature values. Considering the time needed for temperature stabilization, ten to fifteen minutes were necessary before starting the characterization of the monolith once the engine was brought to the selected test point.

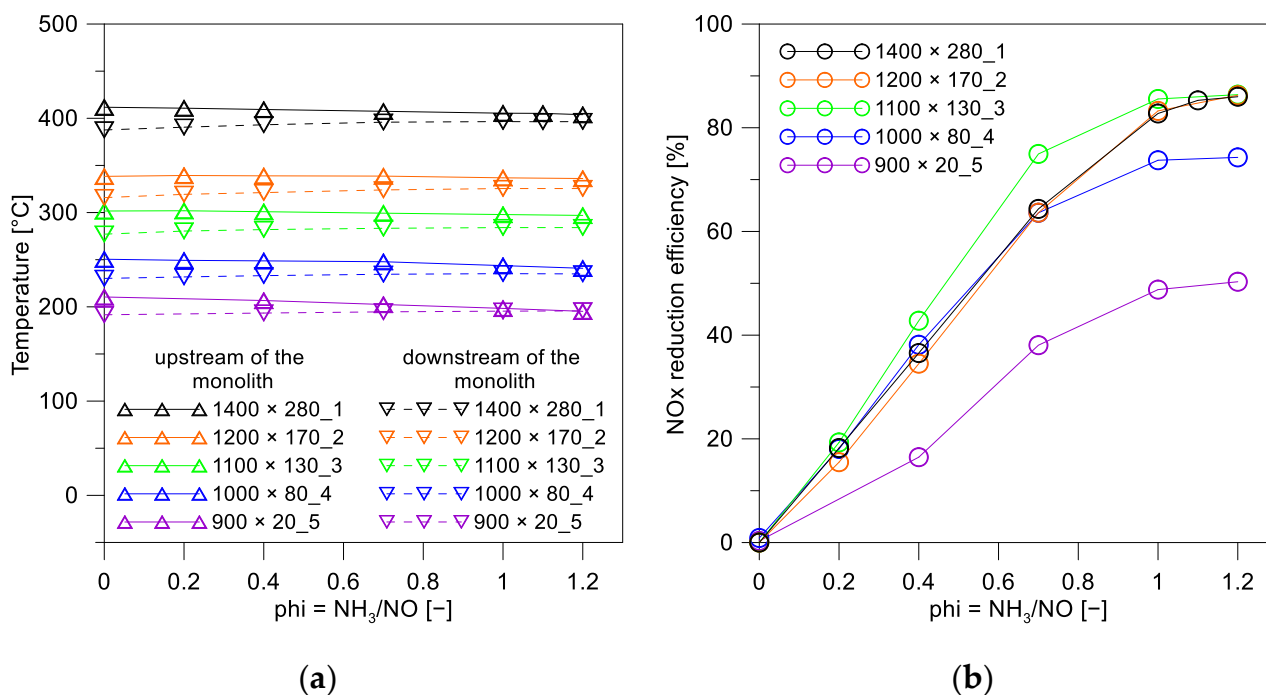


**Figure 9.** (a) Temperature upstream and downstream of the SCR system and (b) NO<sub>x</sub> reduction efficiency as a function of the dosing ratio (phi) with Adblue injection.

Figure 9b shows the NO<sub>x</sub> conversion efficiency versus phi in the five modes. For each mode, the efficiency increased linearly with the dosed quantity. When the stoichiometric condition was reached, a stabilization towards the maximum efficiency value, typical of the prototype under test, was observed. After this value, in fact, the curves reached a plateau.

For mode 5, the efficiency curve was always lower than the other modes. Such behavior was probably due to the very low temperature corresponding to this operating point that inhibited the complete activation of the catalyst, inducing a low reduction efficiency all over the phi sweeps. The low SV and NO<sub>x</sub> concentration, which have a positive effect on NO<sub>x</sub> conversion, were not able to counterbalance the opposite effect of the low temperature.

The low temperature also affected the performance of the monolith in mode 4, although the NO<sub>x</sub> reduction efficiency was, in any case, higher than mode 5 for every value of phi.

Above 300 °C (mode 3-2-1), the curves were higher than modes 4–5, and there was a substantial stabilization of the value of the NO<sub>x</sub> reduction efficiency. The curve relative to mode 3 showed a slightly higher efficiency than modes 1 and 2; this could be ascribable to the lower space velocity, which promotes NO<sub>x</sub> reduction.

Corresponding to phi = 1, the NO<sub>x</sub> reduction efficiency fluctuated between about 50% and 85% depending on the operating conditions. These differences were essentially due to the different temperature of the exhaust gases. Consistently, the lowest efficiency values corresponded to the two modes with the lowest engine load.

The achieved results agreed with the laboratory-scale ones discussed in Section 2, which already identified a good reactivity of the formulation of the tested SCR at relatively low temperatures. Even for temperatures of only 200 °C, the NO<sub>x</sub> reduction capacity was still around 50%.

In a subsequent experimental campaign, gaseous NH<sub>3</sub> was directly injected upstream of the prototype SCR and mixed with the exhaust gases. To this end, a tank of NH<sub>3</sub> in nitrogen was used. The aim of the activity was to evaluate the consistency with the results obtained by injecting AdBlue to confirm that the urea in the AdBlue correctly and completely dissociated in NH<sub>3</sub>, despite the low exhaust gas temperature. Due to limitations in the experimental set-up faced during the test campaign, it was possible to dose the gas mixture only in the modes 3, 4 and 5. At the higher load mode, the amount of NH<sub>3</sub>/N<sub>2</sub> mixture would have been too high to be introduced. Anyway, the main interest of this activity was focused on the lower load modes where the exhaust gas had the minimum temperature.

Gaseous ammonia was directly injected into the exhaust gases and the NO<sub>x</sub> conversion efficiency was measured as a function of the dosing ratio with the same NH<sub>3</sub>/NO values as the previous case. The reduction efficiency showed similar trends.

Figure 10 reports, for phi equal to 1, a comparison of the NO<sub>x</sub> reduction efficiency obtained in the tests carried out with the AdBlue (urea) dosage and when injecting gaseous NH<sub>3</sub>. The comparison was performed in the modes 3–5; very similar results were achieved. The lower efficiency in mode 5 when gaseous ammonia was used was probably due to higher measurement uncertainty for low dosing requests typical of this operating point, mainly in the case of the non-standard NH<sub>3</sub> injection set-up.

It can be concluded that the catalyst test device operated correctly and that the results were specific to the functionality of the SCR prototype tested, also from a quantitative point of view.

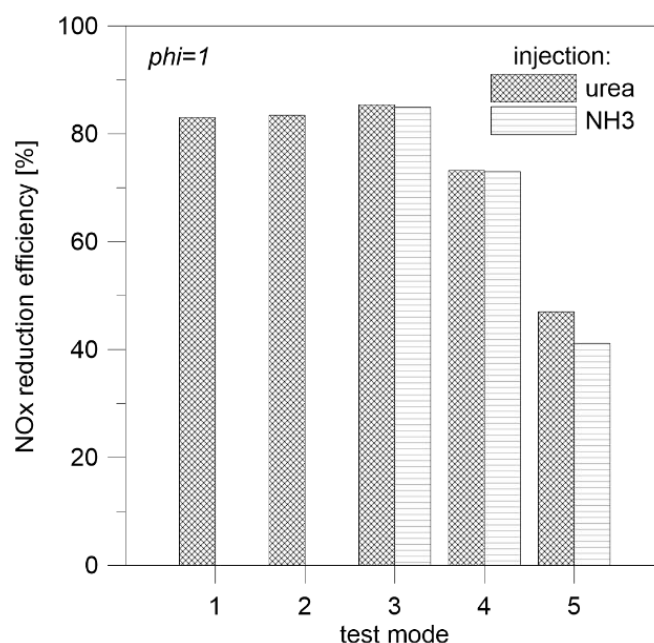


**Figure 10.** NO<sub>x</sub> reduction efficiency at phi = 1 for urea and gaseous NH<sub>3</sub> injection.

#### 4. Conclusions

The comparative study of the monolithic SCR device conducted at the laboratory scale, as a slab and/or as a powder, in terms of its physical-chemical properties and the second step investigating the potentiality offered by the same SCR on an intermediate-scale engine proved to be an original approach of investigation.

The structural, morphological and reduction properties of the monolithic device were revealed as the key parameters governing the NO<sub>x</sub> removal efficiency. The high reducibility of the mixed V-O-W species, synergistically interacting with the titania support, stabilized as an anatase phase, as well as the presence of a vanadium-enriched catalytic surface, were likely the main factors responsible for the NH<sub>3</sub> SCR activity.

The use of the intermediate scale engine revealed a powerful and reliable tool for reproducing the exhaust line conditions that will be encountered by the SCR device in its final installation, reducing the complexity of a test campaign on the real-scale marine engine.

The results of the experimental investigation highlighted the good potentiality of the tested monolith, offering useful insights from a quantitative point of view of a commercial V<sub>2</sub>O<sub>5</sub>-WO<sub>3</sub>-TiO<sub>2</sub> SCR when applied in real working conditions.

The methodological approach corroborated the findings; the engine test results, in fact, were perfectly in agreement with the laboratory-scale ones, already identifying a good reactivity of the formulation of the tested SCR at relatively low temperatures (at 200 °C the NO<sub>x</sub> reduction capacity was still around 50%).

Starting from the obtained results, further studies can be performed with the same method to evaluate the potentiality of proper thermal management or of control strategies in the system optimization in critical conditions, such as a cold-engine start or low load for example.

Moreover, aspects related to the poisoning resistance of the catalytic systems and to ammonia slipping at the exhaust are critical issues to further investigate in the case of marine applications. Considering the well-known issue of the NO<sub>x</sub> reduction efficiency of SCR systems in the case of using fuel with high sulfur content, the authors have also planned an experimental activity, which is currently ongoing, properly devoted to the evaluation of the applicability of such technology in the case of high-Sulfur fuel content in any case lower than 0.5%.

**Author Contributions:** Conceptualization, L.F.L., P.N. and C.G.; methodology, L.F.L., V.L.P., G.P., P.N. and C.G.; validation, L.F.L., G.P., P.N., C.T. and C.G.; investigation, L.F.L., V.L.P., G.P., P.N., C.T. and C.G.; data curation, L.F.L., V.L.P., G.P. and P.N.; writing—original draft preparation, L.F.L., V.L.P. and C.T.; writing—review and editing, L.F.L., V.L.P., G.P., P.N., C.T. and C.G.; visualization, C.T.; supervision, C.B.; project administration, L.F.L., G.P. and P.N.; funding acquisition, L.F.L., G.P. and C.B. All authors have read and agreed to the published version of the manuscript.

**Funding:** This work was funded by the project TECBIA “Tecnologie a Basso Impatto Ambientale per la produzione di energia sui mezzi navali” (Project n. F.090041/01/X36) and by the Project NAUSICA (PON “R&S 2014-2020”, grant n. ARS01\_00334).

**Data Availability Statement:** The data presented in this study are available on request from the corresponding authors.

**Acknowledgments:** The authors are grateful to Luca Pinauda (Hug Engineering AG) for providing the commercial monolithic catalyst. F. Giordano (ISMN-CNR, Italy) and N. Galli (ISMN-CNR, Italy) are kindly acknowledged for technical support in the laboratory and for carrying out XRD and BET analyses, respectively. A. Schiavone (STEMS-CNR, Italy) and S. Alfuso (STEMS-CNR, Italy) are kindly acknowledged for their technical support in setting up the test cell and in the experimental test campaign at the engine test bench.

**Conflicts of Interest:** The authors declare no conflict of interest.

## References

1. Welaya, Y.M.A.; Mosleh, M.; Ammar, N.R. Thermodynamic analysis of a combined gas turbine power plant with a solid oxide fuel cell for marine applications. *Int. J. Nav. Archit.* **2013**, *5*, 529–545. [[CrossRef](#)]
2. George, C.; Ammann, M.; D’Anna, B.; Donaldson, D.J.; Nizkorodov, S.A. Heterogeneous Photochemistry in the Atmosphere. *Chem. Rev.* **2015**, *115*, 4218–4258. [[CrossRef](#)] [[PubMed](#)]
3. Ni, P.; Wang, X.; Li, H. A review on regulations, current status, effects and reduction strategies of emissions for marine diesel engines. *Fuel* **2020**, *279*, 118477. [[CrossRef](#)]
4. Kröcher, O.; Elsener, M.; Jacob, E. A model gas study of ammonium formate, methanamide and guanidinium formate as alternative ammonia precursor compounds for the selective catalytic reduction of nitrogen oxides in diesel exhaust gas. *Appl. Catal. B* **2009**, *88*, 66–82. [[CrossRef](#)]
5. Chen, C.; Cao, Y.; Liu, S.; Chen, J.; Jia, W. Review on the latest developments in modified vanadium-titanium-based SCR catalysts. *Chinese J. Catal.* **2018**, *39*, 1347–1365. [[CrossRef](#)]
6. Lee, C. Performance evaluation of a urea-selective catalytic reduction system in a marine diesel engine. *Proc. Inst. Mech. Eng. Part M J. Eng. Marit. Environ.* **2017**, *231*, 801–808. [[CrossRef](#)]
7. Blatcher, D.J.; Eames, I. Compliance of Royal Naval ships with nitrogen oxide emissions legislation. *Mar. Pollut. Bull.* **2013**, *74*, 10–18. [[CrossRef](#)]
8. Praveena, V.; Martin, M.L.J. A review on various after treatment techniques to reduce NO<sub>x</sub> emissions in a CI engine. *J. Energy Inst.* **2018**, *91*, 704–720. [[CrossRef](#)]
9. Guo, M.Y.; Fu, Z.C.; Ma, D.G.; Ji, N.; Song, C.F.; Liu, Q.L. A short review of treatment methods of marine diesel engine exhaust gases. *Pro. Eng.* **2015**, *121*, 938–943. [[CrossRef](#)]
10. Zhu, Y.; Zhou, W.; Xia, C.; Hou, Q. Application and Development of Selective Catalytic Reduction Technology for Marine Low-Speed Diesel Engine: Trade-Off among High Sulfur Fuel, High Thermal Efficiency, and Low Pollution Emission. *Atmosphere* **2022**, *13*, 731. [[CrossRef](#)]
11. Shi, J.; Zhu, Y.; Peng, H.; Yan, H.; Li, T.; Zhang, J.; Zhou, S. Modeling and simulation of marine SCR system based on Modelica. *Int. J. Engine Res.* **2022**. [[CrossRef](#)]
12. Xia, C.; Zhu, Y.; Zhou, S.; Peng, H.; Feng, Y.; Zhou, W.; Shi, J.; Zhan, J. Simulation study on transient performance of a marine engine matched with high-pressure SCR system. *Int. J. Engine Res.* **2022**. [[CrossRef](#)]
13. Li, W.M.; Liu, H.D.; Chen, Y.F. Promotion of transition metal oxides on the NH<sub>3</sub>-SCR performance of ZrO<sub>2</sub>-CeO<sub>2</sub> catalyst. *Front. Environ. Sci. Eng.* **2017**, *11*, 87–95. [[CrossRef](#)]
14. Guo, M.; Liu, Q.; Zhao, P.; Han, J.; Li, X.; Ha, Y.; Fu, Z.; Song, C.; Ji, N.; Liu, C.; et al. Promotional effect of SO<sub>2</sub> on Cr<sub>2</sub>O<sub>3</sub> catalysts for the marine NH<sub>3</sub>-SCR reaction. *Chem. Eng. J.* **2019**, *361*, 830–838. [[CrossRef](#)]
15. Magnusson, M.; Fridell, E.; Ingelsten, H.H. The influence of sulfur dioxide and water on the performance of a marine SCR catalyst. *Appl. Catal. B* **2012**, *111*, 20–26. [[CrossRef](#)]
16. Lisi, L.; Pirone, R.; Russo, G.; Stanzione, V. Cu-ZSM5 based monolith reactors for NO decomposition. *Chem. Eng. J.* **2009**, *154*, 341–347. [[CrossRef](#)]
17. Moura de Oliveira, M.L.; Silva, C.M.; Tost, R.M.; Farias, T.L.; Lopez, A.J.; Castellon, E.R. A study of copper-exchanged mordenite natural and ZSM-5 zeolites as SCR-NO<sub>x</sub> catalysts for diesel road vehicles: Simulation by neural networks approach. *Appl. Catal. B* **2009**, *88*, 420–429. [[CrossRef](#)]

18. Cheng, Y.; Montreuil, C.; Cavataio, G.; Lambert, C. Sulfur Tolerance and DeSOx Studies on Diesel SCR Catalysts. *SAE Int. J. Fuels Lubr.* **2009**, *1*, 471–476. [[CrossRef](#)]
19. Seo, C.K.; Choi, B. Physicochemical characteristics according to aging of Fe-zeolite and V<sub>2</sub>O<sub>5</sub>-WO<sub>3</sub>-TiO<sub>2</sub> SCR for diesel engines. *J. Ind. Eng. Chem.* **2015**, *25*, 239–249. [[CrossRef](#)]
20. Japke, E.; Casapu, M.; Trouillet, V.; Deutschmann, O.; Grunwaldt, J.D. Soot and hydrocarbon oxidation over vanadia-based SCR catalysts. *Catal. Today* **2015**, *258*, 461–469. [[CrossRef](#)]
21. Zhou, S.; Liu, Y.; Zhu, Y.Q.; Yu, Y.; Li, C.L. Low-Temperature Performances for Monolithic V<sub>2</sub>O<sub>5</sub>-WO<sub>3</sub>/TiO<sub>2</sub> Catalyst in the NH<sub>3</sub>-SCR System. *Asian J. Chem.* **2013**, *42*, 1455–1463. [[CrossRef](#)]
22. Lai, J.-K.; Wachs, I.E. A Perspective on the Selective Catalytic Reduction (SCR) of NO with NH<sub>3</sub> by Supported V<sub>2</sub>O<sub>5</sub>-WO<sub>3</sub>/TiO<sub>2</sub> Catalysts. *ACS Catal.* **2018**, *8*, 6537–6551. [[CrossRef](#)]
23. Zhang, W.; Qi, S.; Pantaleo, G.; Liotta, L.F. WO<sub>3</sub>-V<sub>2</sub>O<sub>5</sub> Active Oxides for NO<sub>x</sub> SCR by NH<sub>3</sub>: Preparation Methods, Catalysts' Composition, and Deactivation Mechanism—A Review. *Catalysts* **2019**, *9*, 527. [[CrossRef](#)]
24. Barrett, E.P.; Joyner, L.G.; Halenda, P.P. The Determination of Pore Volume and Area Distributions in Porous Substances. I. Computations from Nitrogen Isotherms. *J. Am. Chem. Soc.* **1951**, *73*, 373–380. [[CrossRef](#)]
25. García-López, E.I.; Pomilla, F.R.; Megna, B.; Testa, M.L.; Liotta, L.F.; Marci, G. Catalytic Dehydration of Fructose to 5-Hydroxymethylfurfural in Aqueous Medium over Nb<sub>2</sub>O<sub>5</sub>-Based Catalysts. *Nanomaterials* **2021**, *11*, 1821. [[CrossRef](#)] [[PubMed](#)]
26. Yu, W.; Wua, X.; Si, Z.; Weng, D. Influences of impregnation procedure on the SCR activity and alkali resistance of V<sub>2</sub>O<sub>5</sub>-WO<sub>3</sub>/TiO<sub>2</sub> catalyst. *Appl. Surf. Sci.* **2013**, *283*, 209–214. [[CrossRef](#)]
27. Xiao, X.; Xiong, S.; Li, B.; Geng, Y.; Yang, S. Role of WO<sub>3</sub> in NO Reduction with NH<sub>3</sub> over V<sub>2</sub>O<sub>5</sub>-WO<sub>3</sub>/TiO<sub>2</sub>: A New Insight from the Kinetic Study. *Catal. Lett.* **2016**, *146*, 2242–2251. [[CrossRef](#)]
28. Marci, G.; García-López, E.I.; Pomilla, F.R.; Liotta, L.F.; Palmisano, L. Enhanced (photo)catalytic activity of Wells-Dawson (H<sub>6</sub>P<sub>2</sub>W<sub>18</sub>O<sub>62</sub>) in comparison to Keggin (H<sub>3</sub>PW<sub>12</sub>O<sub>40</sub>) heteropolyacids for 2-propanol dehydration in gas-solid regime. *Appl. Catal.* **2016**, *528*, 113–122. [[CrossRef](#)]
29. Besselmann, S.; Freitag, C.; Hinrichsen, O.; Muhler, M. Temperature-programmed reduction and oxidation experiments with V<sub>2</sub>O<sub>5</sub>/TiO<sub>2</sub> catalysts. *Phys. Chem. Chem. Phys.* **2001**, *3*, 4633–4638. [[CrossRef](#)]
30. Wang, C.; Yang, S.; Chang, H.; Peng, Y.; Li, J. Dispersion of tungsten oxide on SCR performance of V<sub>2</sub>O<sub>5</sub>-WO<sub>3</sub>/TiO<sub>2</sub>: Acidity, surface species and catalytic activity. *Chem. Eng. J.* **2013**, *225*, 520–527. [[CrossRef](#)]
31. Ousmane, M.; Liotta, L.F.; Di Carlo, G.; Pantaleo, G.; Venezia, A.M.; Deganello, G.; Retailleau, L.; Boreave, A.; Giroir-Fendler, A. Supported Au catalysts for low-temperature abatement of propene and toluene, as model VOCs: Support effect. *Appl. Catal. B* **2011**, *101*, 629–637. [[CrossRef](#)]
32. Komornicki, S.; Radecka, M.; Sobas, P. Structural properties of TiO<sub>2</sub> ± WO<sub>3</sub> thin films prepared by r.f. sputtering. *J. Mater. Sci. Mater* **2004**, *15*, 527–531. [[CrossRef](#)]
33. Mdlovu, N.V.; Yang, N.C.; Lin, K.S.; Chang, C.J.; Dinh, K.T.; Lin, Y.G. Formulation and characterization of W-doped titania nanotubes for adsorption/photodegradation of methylene blue and basic violet 3 dyes. *Catalysts* **2022**, *388–389*, 36–46. [[CrossRef](#)]
34. Hu, J.; Lei, Y.; Yuan, M.; Lin, Y.; Jiang, Z.; Ouyang, Z.; Du, P.; Wu, Y. Enhanced photoelectric performance of QDs anchored WO<sub>3</sub> with a “dot-on-nanoparticle” structure. *Mater. Res. Express* **2020**, *7*, 075602. [[CrossRef](#)]
35. Zakharova, G.S.; Podval'Naya, N.V.; Kuznetsov, M.V. XPS study of nanorods of doped vanadium oxide M × V<sub>2</sub>O<sub>5</sub> • nH<sub>2</sub>O (M = Na, K, Rb, Cs). *Russ. J. Inorg. Chem.* **2011**, *56*, 267–272. [[CrossRef](#)]
36. Schuhl, Y.; Baussart, H.; Delobel, R.; Le Bras, M.; Leroy, J.-M. Study of Mixed-oxide Catalysts Containing Bismuth, Vanadium and Antimony. *J. Chem. Soc. Faraday Trans.* **1983**, *79*, 2055–2069. [[CrossRef](#)]
37. Chenakin, S.P.; Silvy, R.P.; Kruse, N. X-ray induced surface modification of aluminovanadate oxide. *Catal. Lett.* **2005**, *102*, 39–43. [[CrossRef](#)]
38. Palcheva, R.; Dimitrov, L.; Tyuliev, G.; Spojakina, A.; Jiratova, K. TiO<sub>2</sub> nanotubes supported NiW hydrodesulphurization catalysts: Characterization and activity. *Appl. Surf. Sci.* **2013**, *265*, 309–316. [[CrossRef](#)]
39. Cheng, P.; Deng, C.S.; Liu, D.N.; Dai, X.M. Titania surface modification and photovoltaic characteristics with tungsten oxide. *Appl. Surf. Sci.* **2008**, *254*, 3391–3396. [[CrossRef](#)]
40. Caravaca, M.; Morales, J.J.; Abad, J. Interaction of NO with SiO<sub>x</sub>/TiO<sub>2</sub> (1 1 0)-(1 × 2). *Appl. Surf. Sci.* **2021**, *551*, 2–6. [[CrossRef](#)]
41. Brack, W.; Heine, B.; Birkhold, F.; Deutschmann, O. Formation of Urea-Based Deposits in an Exhaust System: Numerical Predictions and Experimental Observations on a Hot Gas Test Bench. *Emiss. Control Sci. Technol.* **2016**, *2*, 115–123. [[CrossRef](#)]